

*A Hybrid Positive-and-Negative Curvature Approach for Detection of the Edges of Magnetic Anomalies, and Its Application in the South China Sea*

**Lianghui Guo, Rui Gao, Xiaohong Meng & Guoli Zhang**

**Pure and Applied Geophysics**  
pageoph

ISSN 0033-4553  
Volume 172  
Number 10

Pure Appl. Geophys. (2015)  
172:2701–2710  
DOI 10.1007/s00024-014-0956-y

**pure and  
applied  
geophysics**

Vol. 172  
No. 10  
pp. 2481–2960  
2015  
ISSN 0033-4553



pageoph

Birkhäuser

**Your article is protected by copyright and all rights are held exclusively by Springer Basel. This e-offprint is for personal use only and shall not be self-archived in electronic repositories. If you wish to self-archive your article, please use the accepted manuscript version for posting on your own website. You may further deposit the accepted manuscript version in any repository, provided it is only made publicly available 12 months after official publication or later and provided acknowledgement is given to the original source of publication and a link is inserted to the published article on Springer's website. The link must be accompanied by the following text: "The final publication is available at [link.springer.com](http://link.springer.com)".**



## A Hybrid Positive-and-Negative Curvature Approach for Detection of the Edges of Magnetic Anomalies, and Its Application in the South China Sea

LIANGHUI GUO,<sup>1,2</sup> RUI GAO,<sup>2</sup> XIAOHONG MENG,<sup>1</sup> and GUOLI ZHANG<sup>3</sup>

**Abstract**—In work discussed in this paper the characteristics of both the most positive and most negative curvatures of a magnetic anomaly were analyzed, and a new approach for detection of the edges of magnetic anomalies is proposed. The new approach, called the hybrid positive-and-negative curvature approach, combines the most positive and most negative curvatures into one curvature by formula adjustments and weighted summation, combining the advantages of the two curvatures to improve edge detection. This approach is suitable for vertically magnetized or reduction-to-pole anomalies, which avoids the complexity of magnetic anomalies caused by oblique magnetization. Testing on synthetic vertically magnetized magnetic anomalies data demonstrated that the hybrid approach traces the edges of magnetic source bodies effectively, discriminates between high and low magnetism intuitively, and is better than approaches based solely on use of the most positive or most negative curvature. Testing on reduced-to-pole magnetic anomalies data around the ocean basin of the South China Sea showed that the hybrid approach enables better edge detection than the most positive or most negative curvatures. On the basis of the features of the reduced-to-pole magnetic anomalies and their hybrid curvature, we suggest the tectonic boundary between the southwestern subbasin and the eastern subbasin of the South China Sea ranges from the northeastern edge of the Zhongsha Islands in the southeast direction to the northeastern edge of the Reed Bank.

**Key words:** Magnetic anomaly, Edge detection, Curvature, South China Sea.

### 1. Introduction

In the suture zone between plates (or blocks) or the contact zone of different geological bodies or fault zones, the rate of variation of magnetic

anomalies is usually high, because of the substantial magnetism contrasts across these boundaries. It is apparent from the literature that edge detection (or enhancement) of magnetic anomalies is important in determining tectonic or lithological boundaries.

Detection of the edge of a magnetic anomaly is usually based on derivative transformations of the anomaly and its properties, for example zero contours of the vertical derivatives (EVJEN 1936), extreme points of total horizontal derivatives (CORDELL 1979, 1985), or analytical signal amplitudes (NABIGHIAN 1972; ROEST *et al.* 1992). However, when anomalies contain a large range of amplitudes, their horizontal and vertical derivatives will also contain large and small-amplitude responses, making the latter hard to see. MILLER and SINGH (1994) introduced the tilt angle concept, a balanced vertical derivative, which enables good enhancement of both large and small-amplitude anomalies. FEDI and FLORIO (2001) reported use of the horizontal derivative of a weighted sum of anomalies (or their any order derivative) and the vertical derivatives, as an enhanced way of achieving high-resolution edge detection. Later, FEDI (2002) proposed multiscale derivative analysis based on the same procedure to enhance edge detection on different scales. VERDUZCO *et al.* (2004) suggested using the total horizontal derivative of the tilt angle as an edge detector. WIINS *et al.* (2005) developed the theta map, a balanced total horizontal derivative, for detection of edges irrespective of strike and amplitude. COOPER and COWAN (2006) used a horizontal tilt angle, a balanced horizontal derivative, to enhance features with a given orientation. COOPER and COWAN (2008) proposed a normalized standard deviation based on ratios of the windowed standard deviation of anomaly derivatives to detect large and small-

<sup>1</sup> Key Laboratory of Geo-detection, Ministry of Education, China University of Geosciences, Beijing 100083, China. E-mail: guo\_lianghui@163.com

<sup>2</sup> Institute of Geology, Chinese Academy of Geological Sciences, Beijing 100037, China. E-mail: gaorui@cags.ac.cn

<sup>3</sup> Tianjin Center, China Geological Survey, Tianjin 300170, China.

amplitude edges simultaneously. COOPER (2009) suggested balancing the analytical signal amplitude and the profile curvature (MITASOVA and JAROSALAV 1993), by use of orthogonal Hilbert transforms, to improve resolution of edges.

Use of curvature attributes is a popular technique in seismic data interpretation (ROBERTS 2001; CHOPRA and MARFURT 2007; KLEIN *et al.* 2008). They measure the degree of bending of seismic reflections along a surface or in a volume, enabling identification of subtle faults, fractures, and other geological features. The horizontal heterogeneity of magnetism in the subsurface causes variations of magnetic anomaly on the observational surface. Consequently, curvatures of magnetic anomalies, describing how bent a curve or surface is at an arbitrary point, can theoretically be used to reveal lineaments or geological features.

HANSEN and DE RIDDER (2006) analyzed lineaments in aeromagnetic data on the basis of the principal curvature of the total horizontal gradient. PHILLIPS *et al.* (2007) presented a curvature-based approach (using both most negative and most positive curvatures) to locate the sources and estimate their depths and strikes. LI (2008) analyzed the similarities of and differences between seismic attributes and potential-field anomaly transformations and emphasized that only the most positive, most negative, and contour curvatures can be considered in potential field analyses. COOPER (2009) proposed a balanced profile curvature to enhance potential-field anomalies. LEE *et al.* (2013) introduced analysis of full, profile, and plan curvatures for discrimination of the location and type of magnetic sources. CEVALLOS *et al.* (2013) applied several curvature types to airborne gravity gradient data and analyzed the characteristics of mean, differential, Gaussian, and shape index curvatures and their separate use in geological interpretation. However, in the potential-field literature, the curvature-based approach has not yet become a popular technique for detection of the edges of magnetic (and gravity) anomalies.

In the work discussed in this paper, use of the most positive and most negative curvatures for detection of the edges of magnetic anomalies was studied by analyzing the characteristics of the two curvatures of magnetic anomaly caused by the one-prism model. A new hybrid positive-and-negative

curvature approach is proposed as a means of enhancing edge detection. The new approach was tested by using both synthetic magnetic anomaly data and real magnetic data in the South China Sea. The most positive and most negative curvature approaches and the zero contours of second-order vertical derivative approaches were also used to test the data for comparison.

## 2. Method

### 2.1. Most Positive and Most Negative Curvatures

Curvatures of gridded magnetic anomalies can be calculated by fitting a quadratic surface within a moving  $3 \times 3$  window at each grid node (EVANS 1972; ROBERTS 2001; HANSEN and DE RIDDER 2006). First, the quadratic surface is fitted to eight grid nodes surrounding the central grid node, by use of a least-squares approach, as shown in Fig. 1 (EVANS 1972):

$$f(x,y) = Ax^2 + By^2 + Cxy + Dx + Ey + F, \quad (1)$$

where,  $f(x, y)$  is magnetic anomaly data, and  $A, B, C, D, E$ , and  $F$  are coefficients along different directional gradients determined from the  $3 \times 3$  window.

The six coefficients in Eq. (1) can be calculated by use of the following arithmetic expressions (ROBERTS 2001):

$$A = \frac{1}{2} \frac{d^2 f}{dx^2} = \frac{f_1 + f_3 + f_4 + f_6 + f_7 + f_9}{12\Delta x^2} - \frac{f_2 + f_5 + f_8}{6\Delta x^2}, \quad (2)$$

$$B = \frac{1}{2} \frac{d^2 f}{dy^2} = \frac{f_1 + f_2 + f_3 + f_7 + f_8 + f_9}{12\Delta y^2} - \frac{f_4 + f_5 + f_6}{6\Delta y^2}, \quad (3)$$

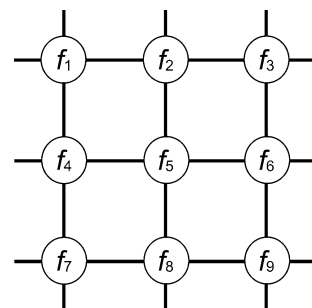


Figure 1  
 $3 \times 3$  grid cell

$$C = \frac{d^2f}{dxdy} = \frac{f_3 + f_7 - f_1 - f_9}{4\Delta x \Delta y}, \quad (4)$$

$$D = \frac{df}{dx} = \frac{f_3 + f_6 + f_9 - f_1 - f_4 - f_7}{6\Delta x}, \quad (5)$$

$$E = \frac{df}{dy} = \frac{f_1 + f_2 + f_3 - f_7 - f_8 - f_9}{6\Delta y}, \quad (6)$$

$$F = \frac{2(f_2 + f_4 + f_6 + f_8) - (f_1 + f_3 + f_7 + f_9) + 5f_5}{9}, \quad (7)$$

where  $f_1-f_9$  refer to the grid node values of the magnetic anomaly shown in Fig. 1, and  $\Delta x$  and  $\Delta y$  are the grid intervals in the  $x$  and  $y$  directions, respectively.

By using the above coefficients, ROBERTS (2001) defined the following curvature attributes for seismic data interpretation: mean, Gaussian, maximum, minimum, most positive, most negative, dip, strike, contour curvatures, curvedness and shape index. Each curvature attribute accentuates different geological features, and they are usually analyzed together for comprehensive interpretation.

Herein, the most positive curvature ( $k_{\text{pos}}$ ) and the most negative curvature ( $k_{\text{neg}}$ ) are defined by Eqs. (8) and (9) respectively:

$$k_{\text{pos}} = (A + B) + \sqrt{(A - B)^2 + C^2}, \quad (8)$$

$$k_{\text{neg}} = (A + B) - \sqrt{(A - B)^2 + C^2}. \quad (9)$$

In seismic data interpretation,  $k_{\text{pos}}$  exaggerates both faults and smaller linear features on the surface (ROBERTS 2001), and  $k_{\text{neg}}$  has a similar geological implication. In practice, these two curvature attributes are usually analyzed with other attributes for better interpretation.

To understand the characteristics of most positive and most negative curvatures in magnetic fields, the two curvatures of a vertically magnetized magnetic anomaly (Fig. 2a) caused by a high-magnetization prism were calculated by use of Eqs. (8) and (9); the results are shown in Fig. 2b, c, respectively, in which the most positive and most negative curvatures are normalized. The  $k_{\text{pos}}$  map presents negative values inside the prism, implying high magnetization, whereas positive values outside the prism indicate low magnetization. The transition of values from positive to negative in the  $k_{\text{pos}}$  map, i.e., near the zero contour, approximately corresponds to edge of the prism. However, higher positive values exist at the outer corners of the prism, disturbing correct recognition of the entire edge of the prism. The  $k_{\text{neg}}$  map also has negative values inside the prism, implying high magnetization, and low negative values (rather than positive values) outside the prism. The transition of values from positive to negative in the  $k_{\text{neg}}$  map is far from the edge of the prism. Higher negative values occur at the inner corners of the prism, affecting correct tracing of the entire edge of the prism. Unlike the  $k_{\text{pos}}$  map dominated by the positive

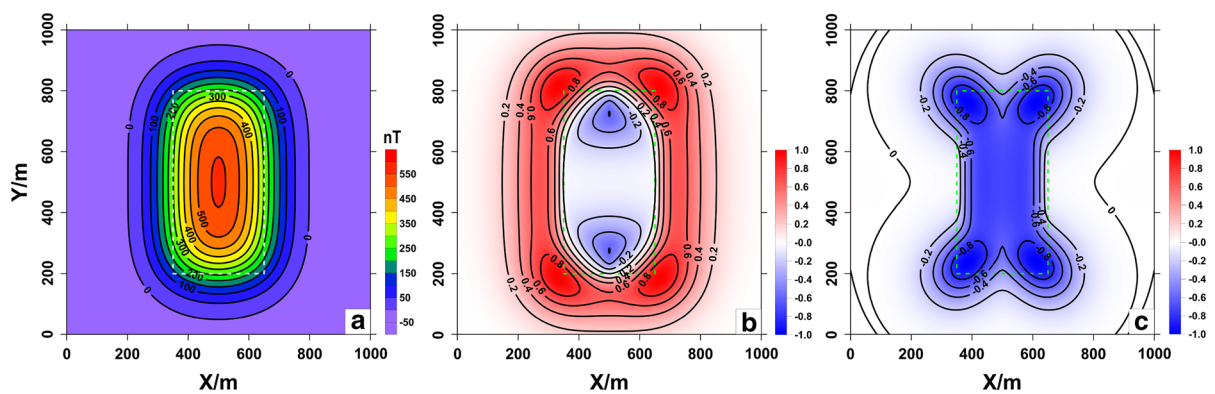


Figure 2

a Vertically magnetized magnetic anomaly of a prism, b normalized most positive curvature, and c normalized most negative curvature. The white dotted box in a and the green dotted boxes in b and c represent the true edge of the prism

values, the  $k_{\text{neg}}$  map is dominated by the negative values. Therefore, the positive and negative values of both curvatures could be used to qualitatively distinguish low and high magnetization of lithology, and the transition of values from positive to negative could be adopted to approximately trace anomaly edges despite of disturbance of the higher values at the corners. This should be done by integrating the two curvatures, rather than using each single curvature in isolation.

## 2.2. Hybrid Positive-and-Negative Curvature

To improve use of the most positive and most negative curvatures for detection of the edges of magnetic anomalies, we associated both curvatures and proposed a new curvature approach, herein called as the hybrid positive-and-negative curvature. The calculation procedure for this approach is described as follows:

1. Replace all the negative values of  $k_{\text{pos}}$  in Eq. (8) with zero values, to take advantage of use of the positive values of  $k_{\text{pos}}$  for revealing low magnetization of the lithology:

$$\begin{cases} \text{when } k_{\text{pos}} \geq 0, k_{\text{pos}} = k_{\text{pos}} \\ \text{when } k_{\text{pos}} < 0, k_{\text{pos}} = 0 \end{cases}. \quad (10)$$

2. Replace all the positive values of  $k_{\text{neg}}$  in Eq. (9) with zero values, to take advantage of use of the negative values of  $k_{\text{neg}}$  for revealing high magnetization of the lithology:

$$\begin{cases} \text{when } k_{\text{neg}} \leq 0, k_{\text{neg}} = k_{\text{neg}} \\ \text{when } k_{\text{neg}} > 0, k_{\text{neg}} = 0 \end{cases}. \quad (11)$$

3. Calculate the weighted sum  $k_{\text{sum}}$  of the renewed  $k_{\text{pos}}$  in step (1) and the renewed  $k_{\text{neg}}$  in step (2), to organically fuse the virtues of  $k_{\text{pos}}$  and  $k_{\text{neg}}$  in distinguishing lithology and enhancing edge detection:

$$k_{\text{sum}} = w_p k_{\text{pos}} + w_n k_{\text{neg}}, \quad (12)$$

where  $w_p$  and  $w_n$  are positive weight coefficients for the renewed  $k_{\text{pos}}$  and renewed  $k_{\text{neg}}$ , respectively. These two weighted coefficients control the effect of each of  $k_{\text{pos}}$  and  $k_{\text{neg}}$  in the hybrid curvature, where  $w_p + w_n = 1$ . If  $w_p > w_n$ ,  $k_{\text{pos}}$  will have a greater effect, and vice versa.

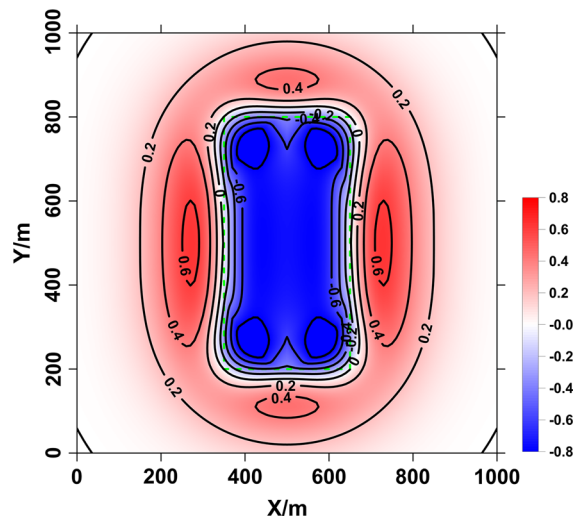


Figure 3  
a Hybrid positive-and-negative curvature of the magnetic anomaly in Fig. 2a. The green dotted box represents the true edge of the prism

4. Divide  $k_{\text{sum}}$  in step (3) by the maximum of its absolute value, to yield a new normalized curvature, i.e., the hybrid positive-and-negative curvature  $k_{\text{pn}}$ :

$$k_{\text{pn}} = k_{\text{sum}} / \max(\text{abs}(k_{\text{sum}})), \quad (13)$$

where  $\max(\text{abs}(k_{\text{sum}}))$  is the maximum of the absolute value of  $k_{\text{sum}}$ .

With the above procedure, the hybrid curvature of the vertically magnetized magnetic anomaly of the prism (Fig. 2a) was calculated; the result is shown in Fig. 3. Both  $w_p$  and  $w_n$  in Eq. (12) were simply set as 0.5. Similar to the  $k_{\text{pos}}$  and  $k_{\text{neg}}$  maps, the  $k_{\text{pn}}$  map presents negative values inside the prism, implying high magnetization, and positive values outside the prism, indicating low magnetization. In the  $k_{\text{pn}}$  map, positive values have almost the same magnitude as negative values, which enables high and low magnetization of the lithology to be distinguished intuitively and clearly. Transition of the values from positive to negative (especially the zero contour) in the  $k_{\text{pn}}$  map coincides well with the edge of the prism, indicating better edge detection by the hybrid curvature than by either the most positive curvature or the most negative curvature separately.

Note that derivatives are involved in calculation of most positive and most negative curvatures and the

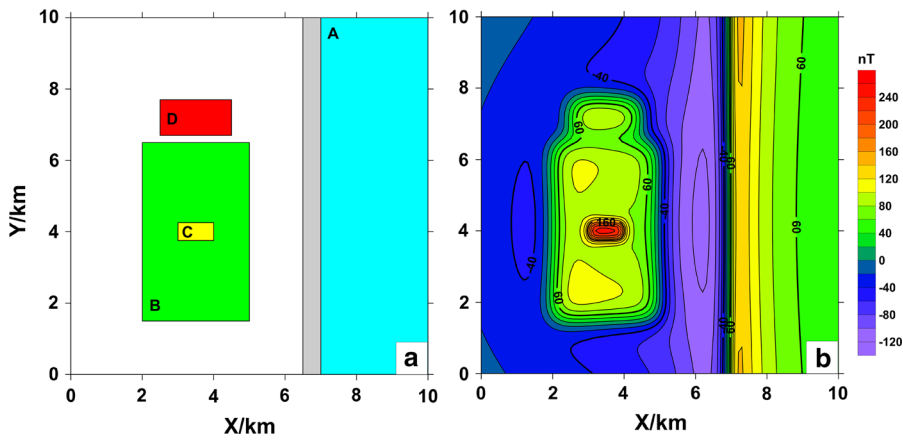


Figure 4

a Outline of each body of the synthetic model projected on to the horizontal plane, b theoretical vertically magnetized magnetic anomalies

hybrid approach. Consequently, data denoising is necessary before calculation of these curvatures when anomaly data are contaminated by noise. Also note that oblique magnetization usually causes complexity of the total magnetic intensity (TMI) anomalies. Hence, reduction to the pole (RTP) of the TMI data is necessary before calculation of these curvatures.

### 3. Data Experiments

#### 3.1. Test on Synthetic Data

The test model consisted of four bodies: one large step A on the right, one large cuboid B with one small cuboid C in the center, and one medium cuboid D at the top left (Fig. 4a). The flank of step A is inclined to the left, making its edges vary with depth. Cuboid B is overlain by cuboid C, resulting in superimposed anomalies, and is adjacent to cuboid D, resulting in interfering anomalies. The geometry of the model included a  $101 \times 101$  regular grid with grid spacing of 100 m along both X-axis and Y-axis. Forward modeling was conducted for vertically magnetized magnetic anomalies on a flat surface with an elevation of 0 m. Figure 4b shows the map of the theoretical vertically magnetized magnetic anomalies of the model.

Edge detection was then conducted on the theoretical magnetic anomalies using the most positive, most negative, and hybrid curvature approaches; the

results are shown in Fig. 5. Figure 6 shows the results along the profiles of  $X = 3.5$  km and  $Y = 4$  km. In this case, the most positive and most negative curvatures were normalized, and both  $w_p$  and  $w_n$  in Eq. (12) were simply set to 0.5. The  $k_{\text{pos}}$  map is dominated by positive values outside each body, indicative of low magnetization, whereas the  $k_{\text{neg}}$  map is dominated by negative values inside each body, implying high magnetization. The transition of values from positive to negative in the  $k_{\text{pos}}$  and  $k_{\text{neg}}$  maps coincides well with the upper edge of step A, but does not coincide well with the lower edge of step A and the edges of cuboids B, C, and D, especially at their corners. However, the  $k_{\text{pn}}$  map presents negative values inside each body and positive values outside each body, of almost the same magnitude, distinguishing high and low magnetization of the lithology intuitively and clearly. The transition of values from positive to negative (especially zero contours) in the  $k_{\text{pn}}$  map coincides well with the edges of each body except for the bottom edge of step A, indicative of effective enhancement of edge detection.

Because second-order derivatives are used in the calculation of the most positive and most negative curvatures and the hybrid curvature, detection of the edges of theoretical magnetic anomalies was also conducted by using the conventional approach of the second-order vertical derivative (2nd VD) for comparison. Figure 7 shows the map of the zero contours of the 2nd VD of the theoretical magnetic anomalies. Around the edges of all bodies, the zero contours of

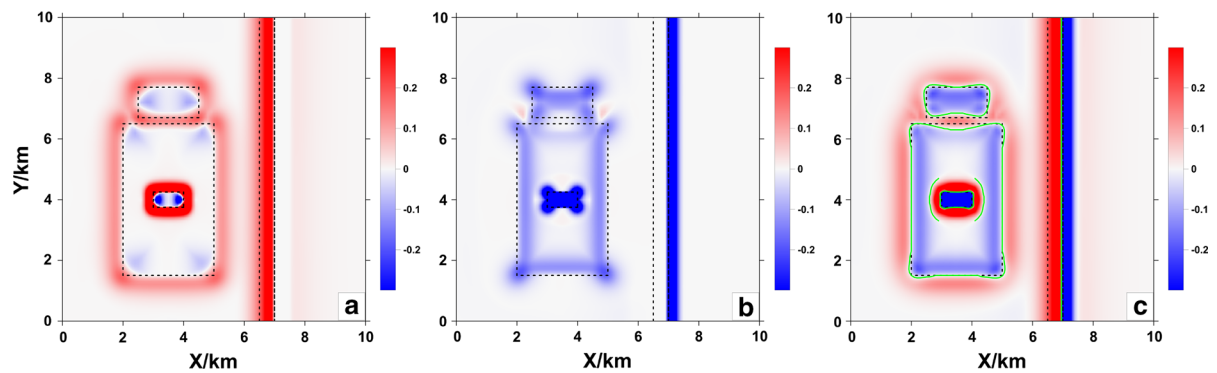


Figure 5

**a**, **b**, and **c**, respectively, show normalized most positive curvature, normalized most negative curvature, and the hybrid curvature of the theoretical magnetic anomalies. The *dotted black lines* outline the true edge of each body. The *green solid lines* in **c** represent zero contours of the hybrid curvature

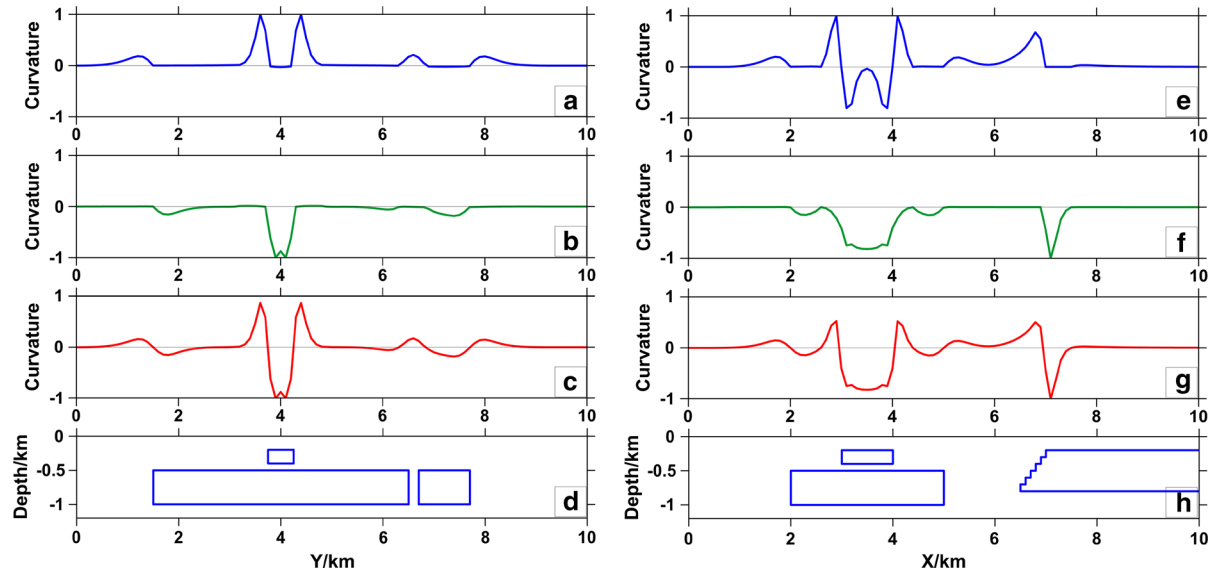


Figure 6

**a**, **b**, and **c**, respectively, show normalized most positive curvature, normalized most negative curvature, and the hybrid curvature of the theoretical magnetic anomalies along the profiles of  $X = 3.5$  km; **e**, **f**, and **g** show those along the profiles of  $Y = 4$  km; **d** and **h** Separately show the outline of each body along the panels of  $X = 3.5$  km and  $Y = 4$  km

the 2nd VD coincide well with the edges of each body, similar to the zero contours in the  $k_{pn}$  map (green curves in Fig. 5c). But beyond that, serious high-frequency noise occurs in the zero contours of the 2nd VD, disturbing detection of its edge.

### 3.2. Test on Real Data in the South China Sea

The South China Sea (SCS) is one of the largest marginal seas in the Western Pacific, located at the convergence of the Eurasian plate, the Pacific plate,

the Philippine Sea Plate, and the Indian–Australian plate. It evolved as a result of the interaction of these major tectonic plates and Cenozoic sea floor spreading (TAYLOR and HAYES 1980, 1983; BRIAIS *et al.* 1993). On the basis of magnetic anomalies and other scientific data, BRIAIS *et al.* (1993) suggested that the ocean basin of the SCS underwent sea floor spreading twice. Rifting in the NW–SE direction occurred in the SCS during 32–30 Ma, and then spreading of the first sea floor in the N–S direction occurred during 30–26 Ma, forming the northern and southern

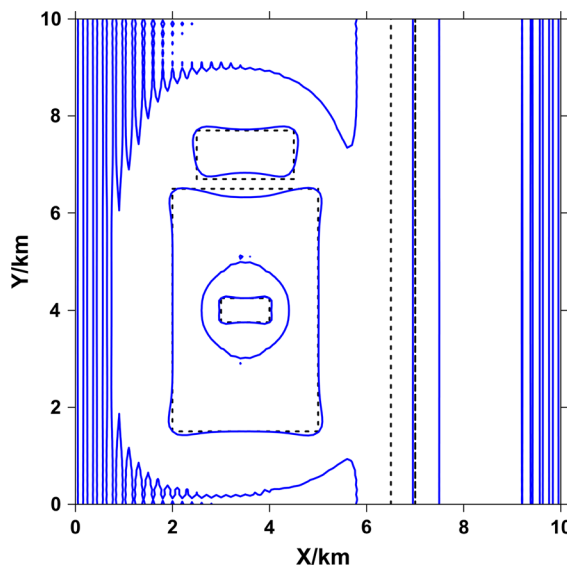


Figure 7

Second-order vertical derivative of the magnetic anomalies of the model. The dotted black lines outline the true edge of each body. The blue solid lines show zero contours of the second-order vertical derivative

oceanic crusts of the eastern subbasin. From 26 to 24 Ma, the spreading axis shifted toward the south. After that, the second sea floor spreading event in the NW–SE direction occurred during 24–15.5 Ma, forming the southwestern subbasin and the middle part of the eastern subbasin of the SCS.

The tectonic boundary between the southwestern and eastern subbasins is an important boundary in the ocean basin of the SCS. It is crucial to understanding the sea floor spreading pattern of the ocean basin. Several teams of researchers have suggested that this tectonic boundary may be a fault zone, often referred to as the Zhongnan fault zone in the Chinese literature (YAO *et al.* 1994; LI *et al.* 2008), trending nearly north–south from the eastern edge of the Zhongsha Islands (Macclesfield Bank) to the western edge of the Reed Bank (TAYLOR and HAYES 1983; NISSEN and HAYES 1995; YAO *et al.* 1994; TRUNG *et al.* 2004; LI *et al.* 2008; SUN *et al.* 2009). However, LI *et al.* (2011) and FRANKE (2013) suggested it was a fracture zone trending northwest–southeast from the eastern edge of the Zhongsha Islands to the eastern edge of the Reed Bank. One important cause of this different understanding is that the magnetic survey lines in the transition area

between the southwestern subbasin and the eastern subbasin are sparse, and the magnetic data are of poor quality (LI *et al.* 2011) and severely affected by seamounts and other magmatite sources.

We assembled the total magnetic intensity (TMI) data around the southwestern and eastern subbasins of the SCS from the database of the Magnetic Anomaly Map of East Asia, which was compiled by the Geological Survey of Japan and Coordinating Committee for Coastal and Offshore Geosciences Programmes in East and Southeast Asia (CCOP 1996). Although the original data are from a variety of different magnetic measurements, at different times, with different scales, and with different amounts of noise suppression, the coverage and accuracy of this new compilation are remarkable (LI *et al.* 2008). They are suitable for studies of tectonics and crustal structure. Figure 8 shows the assembled TMI anomalies in the studied area with a grid spacing of 0.05°, superimposed on the topographic map of the seabed.

Because the studied area is located at low magnetic latitudes with a large north–south span, changes in the geomagnetic field direction are large (in this case, magnetic inclination ranges from 6.8° to

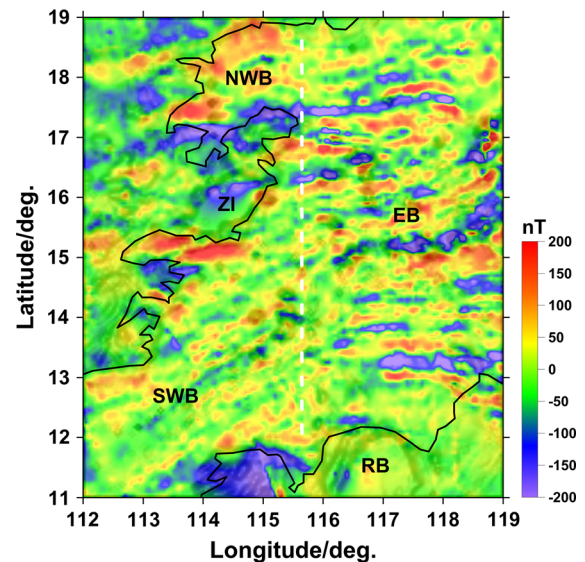


Figure 8

The real total magnetic intensity anomalies around the southwestern and eastern subbasins of the SCS. Black solid lines, continent-and-ocean boundary; white dotted line, Zhongnan fault zone (SUN *et al.* 2009). EB eastern subbasin, SWB southwestern subbasin, NWB northwestern subbasin, ZI Zhongsha Islands, RB Reed Bank

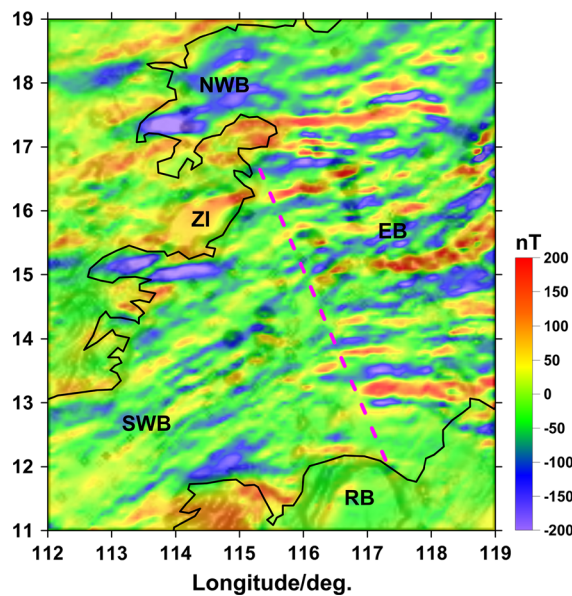


Figure 9

RTP anomalies in the studied area. Black solid lines, continent-and-ocean boundary; pink dotted line, the deduced tectonic boundary between the southwestern subbasin and the eastern subbasin. EB eastern subbasin, SWB southwestern subbasin, NWB northwestern subbasin, ZI Zhongsha Islands, RB Reed Bank

24.7° and magnetic declination ranges from  $-1.7^\circ$  to  $-0.1^\circ$ ). As a result, it is difficult to use the TMI anomalies directly for tectonic studies. By neglecting the effects of remanence, we performed reduction to the pole (RTP) on the TMI anomalies to transform oblique magnetization into vertical magnetization, and thus eliminate the complexity of the TMI

anomalies caused by oblique magnetization. The antisymmetric factor approach with a variable magnetic inclination algorithm proposed by GUO *et al.* (2013b) was adopted to perform the RTP. The preferential filtering approach (Guo and Meng 2013a) was also used to suppress high-frequency noise in the TMI anomalies. Figure 9 shows the resulting RTP anomalies in the studied area superimposed on the topographic seabed map.

The RTP anomalies have different features from east to south in the ocean basin. On the east side the anomalies are strong and the magnetic lineaments strike nearly east–west, whereas on the west side the anomalies are weak and the magnetic lineaments mostly trend northeast–southwest. The boundary of differentiation of these features is clear and just ranges from the northeastern edge of the Zhongsha Islands running in the southeast direction to the northeastern edge of the Reed Bank (Fig. 9, pink dotted line), implying that the magnetic structure and tectonic features of the crust are different on each side of this boundary. From this it can be deduced that this is the tectonic boundary between the southwestern subbasin and the eastern subbasin. The basin on its west side belongs to the southwestern subbasin whereas that on its east side belongs to the eastern subbasin.

To clearly reveal the lineaments (or linear structures) of the RTP anomalies and subsequently to further confirm the tectonic boundary as deduced

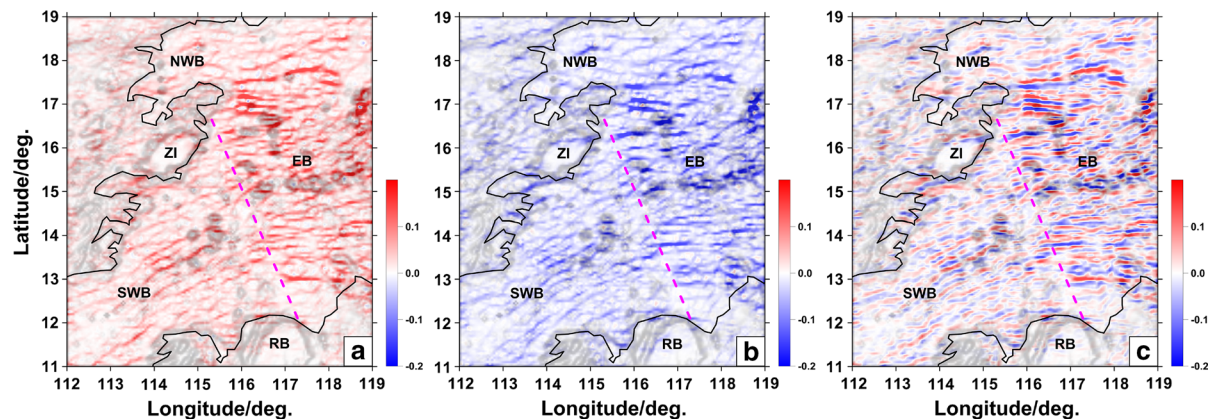


Figure 10

a, b, and c, respectively, show the normalized most positive, normalized most negative, and hybrid curvatures of the RTP anomalies. Black solid lines, continent-and-ocean boundary; pink dotted line, deduced tectonic boundary between the southwestern subbasin and the eastern subbasin. EB eastern subbasin, SWB southwestern subbasin, NWB northwestern subbasin, ZI Zhongsha Islands, RB Reed Bank

above (Fig. 9, pink dotted line), the most positive curvature, most negative curvature, and hybrid curvature of the RTP anomalies were calculated; the results are shown in Fig. 10, in which the most positive and most negative curvatures are normalized, and both  $w_p$  and  $w_n$  in Eq. (12) were simply set as 0.5 for calculation of the hybrid curvature. Details of the lineaments are presented for all three types of curvature. The  $k_{\text{pos}}$  map (Fig. 10a) is dominated by positive values whereas the  $k_{\text{neg}}$  map (Fig. 10b) is dominated by negative values. The  $k_{\text{pn}}$  map (Fig. 10c) shows the positive and negative values side by side with comparable magnitude, presenting clearer and more complete lineaments than the  $k_{\text{pos}}$  and  $k_{\text{neg}}$  maps. In the  $k_{\text{pn}}$  map, the lineaments between the two sides of the above deduced boundary (pink dotted line in Fig. 10c) are distinct from each other. On the east side, the lineaments were found to be of strong magnitude and trend nearly east–west, whereas on the west side the lineaments are of relatively weak magnitude and strike mostly from northeast to southwest. These results are indicative of different magnetic structure and tectonic features in the crust on each side of this boundary. Therefore, the  $k_{\text{pn}}$  map of the RTP anomalies proves that the deduced boundary (pink dotted line in Fig. 10c) corresponds with the tectonic boundary between the southwestern subbasin on the west side and the eastern subbasin on the east side.

#### 4. Conclusions

A hybrid positive-and-negative curvature approach for detection of the edges of magnetic anomalies is presented in this paper. This approach fuses the advantages of the most positive and most negative curvatures to distinguish lithology and enhance edge detection. The detailed procedure used to apply this approach is provided. Because of the complexity of magnetic anomalies caused by oblique magnetization, it is suggested this approach is performed on vertically magnetized or RTP anomalies. The validity of the new hybrid approach was evaluated by use of synthetic data and real magnetic data in the South China Sea. The results indicated that the hybrid approach provides better edge detection than

the conventional most positive and most negative curvatures. The new approach also produces adequate information for distinguishing high and low-magnetism lithology intuitively. The hybrid curvature features of the RTP anomalies in the SCS suggests that the tectonic boundary between the southwestern subbasin and the eastern subbasin ranges from the northeastern edge of the Zhongsha Islands running in the southeast direction to the northeastern edge of the Reed Bank.

It should be noted that similar to the most positive and most negative curvatures and other derivative-based approaches discussed in the Sect. 1, the new hybrid approach is also sensitive to noise and interference effects. Therefore, in practical applications, denoising or separation of anomalies is necessary. Proper understanding of geology and careful analysis will still be of vital importance in successful interpretation of magnetic anomalies.

#### Acknowledgments

We thank the Editor Marek Lewandowski and two anonymous reviewers for their helpful comments and valuable suggestions. We are grateful for financial support from the SinoProbe projects (SinoProbe-02-01 and SinoProbe-01-05), the National Natural Science Foundation of China (41374093, 41104056), the national 863 Project (2014AA06A613), the Geological Survey Project (12120113061600), the Beijing Higher Education Young Elite Teacher Project (YETP0650), and the Fundamental Research Funds for the Central Universities and China postdoctoral science foundation projects (2012M520348).

#### REFERENCES

- BRIAS, A., PATRIAT, P., and TAPPONNIER, P., 1993. *Updated interpretation of magnetic anomalies and seafloor spreading in the South China Sea: implications for the Tertiary Tectonics of Southeast Asia*. J. Geophys. Res., 98(B4), 6299–6328.
- CEVALLOS, C., KOVAC, P., and LOWE, S.J., 2013. *Application of curvatures to airborne gravity gradient data in oil exploration*, Geophysics, 78, G81–G88.
- CHOPRA, S., and MARFURT, K., 2007. *Curvature attribute applications to 3D surface seismic data*, The Leading Edge, 26, 404–414.
- CORDELL, L., 1979. Gravimetric expression of graben faulting in Santa Fe country and the espanola basin, New Mexico. In:

- INGERSOLL, R.V., (Ed.), Guidebook to Santa Fe country: New Mexico Geol. Soc. Guidebook. 30th Field Conference, 59–64.
- CORDELL, L., and V. J. S. GRAUCH, 1985, Mapping basement magnetization zones from aeromagnetic data in the San Juan basin: New Mexico, in J. W. Hinze, ed., *The utility of regional gravity and magnetic anomaly maps*, SEG, 181–197.
- COOPER, G.R.J., and COWAN, D. R., 2006, *Enhancing potential field data using filters based on the local phase*. Computers and Geosciences, 32, 1585–1591.
- COOPER, G.R.J., and COWAN, D. R., 2008, *Edge enhancement of potential field data using normalized statistics*, Geophysics, 73, H1–H4.
- COOPER, G.R.J., 2009, *Balancing images of potential-field data*, Geophysics, 74, L17–L20.
- EVANS I.S. 1972. General geomorphometry, derivatives of altitude and descriptive statistics. In: Spatial Analysis in Geomorphology, (ed. R.J. Chorley), pp.36. Methuen, London.
- EVJEN, H.M. 1936. *The place of the vertical gradient in gravitational interpretations*, Geophysics, 1, 127–136.
- FEDI, M., and FLORIO, G., 2001, *Detection of potential field source boundaries by enhanced horizontal derivative method*, Geophysical Prospecting, 49, 40–58.
- FEDI, M., 2002, *Multiscale derivative analysis: A new tool to enhance detection of gravity source boundaries at various scales*, Geophysical Research Letters, 29, 16-1–16-4.
- FRANKE, D., 2013, *Rifting, lithosphere breakup and volcanism: Comparison of magma-poor and volcanic rifted margins*. Marine and Petroleum geology, 43, 63–87.
- GEOLOGICAL SURVEY OF JAPAN AND COORDINATING COMMITTEE FOR COASTAL AND OFFSHORE GEOSCIENCE PROGRAMMES IN EAST AND SOUTHEAST ASIA (CCOP), 1996. *Magnetic anomaly map of East Asia 1:4,000,000 CD-ROM Version*. Digital Geoscience Map 2(P-1).
- GUO, L., and MENG, X., 2013a. *Preferential filtering for gravity anomaly separation*, Computers and Geosciences, 51, 247–254.
- GUO, L., SHI, L., and MENG, X., 2013b. *The antisymmetric factor method for magnetic reduction to the pole at low latitudes*, Journal of Applied Geophysics, 92, 103–109.
- HANSEN, R. O., and deRIDDER, E., 2006, *Linear feature analysis for aeromagnetic data*, Geophysics, 71, L61–L67.
- KLEIN, P., RICHARD, L., and JAMES, H., 2008. *3D curvature attributes: a new approach for seismic interpretation*, First break, 26, 105–112.
- LEE, M., MORRIS, W., LEBLANC, G., and HARRIS, J., 2013. *Curvature analysis to differentiate magnetic sources for geologic mapping*, Geophysical Prospecting, 61(Suppl. 1). 572–585.
- LI, C. F., ZHOU, Z., LI, J., ET AL., 2008. *Magnetic zoning and seismic structure of the South China Sea ocean basin*. Marine Geophysical Researches, 29, 223–238.
- LI, J. B., DING, W. W., GAO, J. Y., ET AL., 2011. *Cenozoic evolution model of the sea-floor spreading in South China Sea: new constraints from high resolution geophysical data*. Chinese Journal of Geophysics (Chinese Edition), 54, 3004–3015.
- LI, X., 2008. *Seismic attributes and gravity and magnetic transformations: The same mathematics under different names for different geophysical data sets*, SEG 78th Annual Meeting Expanded Abstracts, 9–14.
- MILLER, H. G., and SINGH, V., 1994, *Potential field tilt - A new concept for location of potential field sources*, Journal of Applied Geophysics, 32, 213–217.
- MITASOVA, H., and JAROSALAV, H., 1993, *Interpolation by regularized spline with tension: II-Application to terrain modeling and surface geometry analysis*, Mathematical Geology, 25, 657–669.
- NABIGHIAN, M.N., 1972. *The analytic signal of two-dimensional magnetic bodies with polygonal cross-section; its properties and use for automated anomaly interpretation*, Geophysics, 37, 507–517.
- NISSEN, S. S., and HAYES, D. E., 1995. *Gravity, heat flow, and seismic constraints on the processes of crustal extension: North margin of the South China Sea*. J. Geophy. Res., 100, 22447–22483.
- PHILLIPS, J.D., HANSEN, R.O., and BLAKELY R.J., 2007. *The use of curvature in potential-field interpretation*, Exploration Geophysics, 38, 111–119.
- ROBERTS, A., 2001. *Curvature attributes and their application to 3 D interpreted horizons*, First break, 19, 85–100.
- ROEST, W. R., VERHOEF, J., and PILKINGTON, M., 1992, *Magnetic interpretation using the 3-D analytic signal*, Geophysics, 57, 116–125.
- SUN, Z., ZHONG, Z., KEEP, M., ET AL., 2009. *3D analogue modeling of the South China Sea A discussion on breakup pattern*. Journal of Asian Earth Science, 34, 544–556.
- TAYLOR, B., and HAYES, D. E., 1980. The tectonic evolution of the South China Sea Basin. In: Hayes, D. E. (Eds.), 1980, *The tectonic and Geologic Evolution of Southeast Asian Seas and Islands*. Geophys. Monogr. AGU, 23, 89–104.
- TAYLOR, B., and HAYES, D. E., 1983. Origin and history of South China Sea Basin. In: Hayes, D. E. (Eds.), 1983, *The tectonic and Geologic Evolution of Southeast Asian Seas and Islands*. Geophys. Monogr., AGU, 27, 23–56.
- TRUNG, N. N., LEE, S. M., and QUE, B. C., 2004. *Satellite Gravity Anomalies and Their Correlation with the Major Tectonic Features in the South China Sea*. Gondwana Research, 7(2), 407–424.
- VERDUZCO, B., FAIRHEAD, J.D., GREEN, C.M. and MACKENZIE, C., 2004, *The meter reader - New insights into magnetic derivatives for structural mapping*, The Leading Edge, 23, 116–119.
- WIJS, C., PEREZ, C., and KOWALCZYK, P., 2005. *Theta map: edge detection in magnetic data*, Geophysics, 70, 39–43.
- YAO, B. C., ZENG, W. L., HAYES, D. E., ET AL. 1994. *The geological Memoir of Joint Survey of South China Sea by China and USA* (in Chinese). China University of Geosciences Press, Wuhan.

(Received June 18, 2014, revised September 27, 2014, accepted October 8, 2014, Published online November 19, 2014)